Published in final edited form as:
Science. 2012 December 7; 338(6112): 1308–1313. doi:10.1126/science.1228757.

Crystal structure of the calcium release-activated calcium channel Orai

Xiaowei Hou, **Leanne Pedi**, **Melinda M. Diver**, and **Stephen B. Long**
Structural Biology Program Memorial Sloan-Kettering Cancer Center 1275 York Avenue, New York, New York 10065

Abstract

The plasma membrane protein Orai forms the pore of the CRAC channel (calcium release-activated calcium channel) and generates sustained cytosolic calcium signals when triggered by depletion of calcium from the endoplasmic reticulum. The crystal structure of Orai from *Drosophila melanogaster*, determined at 3.35 angstrom resolution, reveals that the calcium channel is comprised of a hexameric assembly of Orai subunits arranged around a central ion pore. The pore traverses the membrane and extends 20 angstroms into the cytosol. A ring of glutamates on its extracellular side forms the selectivity filter. A basic region near the intracellular side can bind anions that may stabilize the closed state. The architecture of the channel differs markedly from other ion channels and gives insight into the principles of selective calcium permeation and gating.

In many cell types, the depletion of calcium ions (Ca^{2+}) stored within the endoplasmic reticulum (ER) causes opening of Ca^{2+}-selective channels in the plasma membrane (1). The resulting influx of Ca^{2+} through these CRAC (Ca^{2+} release-activated Ca^{2+}) channels generates sustained intracellular Ca^{2+} signals, the roles of which are well-appreciated in cells of the immune system where they mediate signaling through B cell, T cell and Fc receptors (1). Although this process of 'store operated Ca^{2+} entry' has been recognized for decades, Orai and STIM, the CRAC channel pore and its regulator, were identified fairly recently (2-7). Orai, located in the plasma membrane, forms the Ca^{2+} pore and there are three Orai proteins in humans (Orai1-3) (8-10). A mutation in Orai1 that renders the channel non-conductive (R91W) (11) causes a form of immune deficiency, underscoring its importance in the immune system (5). STIM is a single-pass membrane protein in the ER that senses the luminal Ca^{2+} concentration. It opens the pore of Orai following Ca^{2+} store depletion, probably via interaction between the cytosolic portions of STIM and Orai, which accumulate at ER-plasma membrane junctions (reviewed in (1, 12)).

Orai proteins constitute a highly conserved ion channel family and have no discernable sequence homology with other ion channels (5-7), suggesting distinctive architecture and mechanisms for selective ion permeation and gating. From sequence analysis, Orai is predicted to have four transmembrane helices (M1-M4). The chemical accessibility and inter-subunit crosslinking of cysteine residues introduced into the channel by mutagenesis predict that residues on the M1 helix contribute to the ion conduction pore (13, 14). Several lines of evidence indicate that Orai channels are multimers, but studies have led to differing conclusions regarding the oligomeric state. Some studies suggest a tetrameric assembly (15-18), while others hint at a higher order oligomer (14) or raise the possibility that the oligomeric state of the channel might change when it is activated by STIM (15, 18).

Address Correspondence to: Stephen B. Long: Memorial Sloan-Kettering Cancer Center Box 414 1275 York Avenue New York, NY 10065 Tel: 212-639-2959 longs@mskcc.org.

Under physiological conditions, where the extracellular [Ca^{2+}] is 1-2 mM, CRAC channels are exquisitely selective for Ca^{2+} ($P_{Ca}/P_{Na} > 1000$) (19). However, when divalent cations are removed from the extracellular solution, the channels become permeant to monovalent cations including sodium (Na^+) (19, 20). Both the Ca^{2+} and monovalent cation currents require activation by STIM and are blocked by gadolinium (Gd^{3+}) and lanthanum (La^{3+}) ions ($K_i < 100$ nM) from the extracellular side (8, 21, 22).

To better understand ion permeation, ion selectivity and gating in CRAC channels, we have determined the crystal structure of Orai from *Drosophila melanogaster*, which shares 73% sequence identity with human Orai1 within its transmembrane region. We have also determined the structure of the non-conductive K163W mutant, corresponding to the R91W mutant in Orai1 that causes immune deficiency in humans. The structures define the architecture of a Ca^{2+} channel, establish principles of its Ca^{2+} selectivity, and give insight into the mechanism of activation by STIM.

Structure determination and channel reconstitution

To obtain well-diffracting crystals of Orai we evaluated the biochemical behavior of ~ 50 orthologs and engineered a variety of protein forms, including truncations and fusions. Crystals that diffracted to 3.35 Å resolution were obtained from a construct (termed $Orai_{cryst}$) spanning residues 132-341 of Orai from *Drosophila melanogaster* in which two non-conserved cysteine residues and two residues in the hypervariable M3-M4 loop were mutated (Supplementary information). The construct corresponds to the conserved region of Orai and contains all regions necessary for activation by STIM (fig. S1) (23-25).

The function of the purified channel protein was tested by reconstituting it into liposomes and using a fluorescence-based assay to monitor ion flux under divalent ion-free conditions (Fig. 1). As would be expected for a closed channel prior to activation by STIM, ion flux was not detected for $Orai_{cryst}$ or for the K163W mutant. Introduction of the mutation V174A (V102A in Orai1), which creates channels that are open in the absence of STIM (26), yielded a robust decrease in fluorescence, indicative of ion flux (Fig. 1B). We confirmed that the fluorescence decrease was due to ion flux through Orai by adding the pore-blocker Gd^{3+}, which eliminated the observed flux through the pore but had no effect on the baseline fluorescence induced by the Na^+-ionophore monensin. The reconstituted protein therefore recapitulated known properties of Orai.

The crystals form in the space group $P2_13$ and contain two Orai subunits (referred to as subunits A and B of the channel) within the asymmetric unit. Experimental phases were derived from diffraction data collected from crystals containing mercury, iridium and gadolinium heavy atoms. The phases, which were improved by non-crystallographic symmetry averaging, yielded an electron density map that allowed placement of the majority of the amino acid side chains (fig. S2). The atomic model contains amino acids 144 – 334 of Orai except for the M1-M2 loop (amino acids 181 - 190), the M2-M3 loop (amino acids 220 - 235), and amino acids 330 - 334 of subunit B, which are disordered. Anomalous difference electron density peaks for sulfur atoms of methionine and cysteine residues confirm the correct assignment of amino acids in the atomic model (fig. S2E), which is refined to an R_{free} value of 28% (table S1).

Architecture of Orai

The crystal structure shows that the channel is formed from a hexamer of six Orai subunits arranged around a central axis (Fig. 2). Crosslinking and light-scattering data are consistent with a hexameric assembly for both purified Orai in detergent and Orai expressed in cell membranes (fig. S3). Each subunit contains four transmembrane α-helices (M1-M4) and a

helix following M4 that extends into the cytosol (termed the M4 extension helix). The M4 extension helices of neighboring subunits adopt one of two alternating conformations and pack with each other in pairs, giving this region of the channel three-fold symmetry (Fig. 2). Within the channel's transmembrane region, there is six-fold symmetry.

The ion pore is located at the center of the channel along the six-fold axis and the transmembrane helices are arranged in three concentric rings (Fig. 2B). Six M1 helices, one from each subunit, comprise an inner ring of helices and line the ion pore. The M2 and M3 helices constitute a middle ring that surrounds the transmembrane portion of the M1 helices and separates them from M4 helices, which are arranged in an outer ring and located at the periphery of the channel. The channel extends just beyond the extracellular side of the membrane and the M1 helix and the M4 extension helix protrude 20-25 Å into the cytosol.

The M1 helices extend from Thr 144 to Glu 180 and are ~ 55 Å long. The region of M1 that extends into the cytosol was not expected to be part of M1 from sequence analysis and comprises four helical turns at its N-terminus (~ residues 144-157). As this region does not make contacts with other parts of the channel in the structure, it could conceivably interact with cellular factors such as STIM.

The M2 helix traverses just beyond the thickness of a lipid bilayer and the M3 helix extends about two helical turns further into the cytosol. The arrangement of the M2 and M3 helices in a ring surrounding the transmembrane portion of the M1 helices, while leaving the cytosolic portion of M1 free, suggests that M2 and M3 help provide structural integrity to the transmembrane region of the pore but would permit widening of the intracellular region of the pore.

The M4 helices are located furthest away from the ion pore. In comparison to the M1-M3 helices, they have fewer contacts with other parts of the channel and their peripheral location may allow mobility (Fig. 2A). A bend near the middle of the transmembrane region (Pro 288) means that approximately half of M4 (within the outer leaflet) is roughly perpendicular to the plane of the membrane, while the other half is oriented diagonally (Fig. 2A). Connected to M4 by a highly conserved hinge region (residues 305–308), the M4 extensions of subunit A and subunit B pair with one another through an antiparallel coiled-coil helix packing arrangement (Fig. 2C). The interaction involves two residues from each subunit (Ile 316 and Leu 319) that form a hydrophobic patch on the M4 extension, which is otherwise predominantly decorated with hydrophilic amino acids. Mutation of either residue (L273S or L276D mutants of Orai1) disrupts interaction with STIM and its ability to open the channel (27-29).

Chemical composition of the pore

The chemical environment along the length of the ion pore is determined by the M1 side chain residues that line it. This is in marked contrast to the pore of K^+ channels where a substantial part of it is formed by an extended conformation of the polypeptide backbone (30). The Orai pore has four distinct sections (Fig. 3A and B): (i) a ring of glutamates at its extracellular end (termed the glutamate ring and comprised of six Glu 178 side chains), (ii) a hydrophobic section spanning three helical turns of M1 within the transmembrane region, (iii) a basic section spanning three helical turns near the intracellular side, and (iv) a wider section that extends into the cytosol.

The pore is ~ 55 Å long and its diameter varies along its distance (Fig. 3B). In the glutamate ring, the Glu 178 side chains point toward the center of the pore with their side chain oxygen atoms separated by ~ 6.5 Å across it, giving the extracellular entrance to the pore negative

electrostatic potential (Fig. 3B and C). Glu 178, which is conserved in Orai channels, is the only acidic residue lining the pore (31).

The side chains of Val 174, Phe 171, and Leu 167 are separated by 8 – 10 Å across the pore and line the walls of the hydrophobic section, which is roughly tube-shaped and ~ 18 Å long (Fig 3B). The hydrophobic side chains are well packed in the pore, make extensive van der Waals interactions with one another, and are strictly conserved among Orai channels. This region also has well-defined electron density (fig. S2) and has the lowest temperature factors of the structure, suggesting that it is relatively rigid. In addition to lining the pore, the hydrophobic residues form a core of the protein that likely contributes to the channel's structural integrity. Mutations of amino acids in the hydrophobic region have yielded channels with dramatically altered ion conduction properties. For instance, mutations of Val 174 (Orai1 mutants V102C, V102A, V102T, or V102S) or Gly 170 (Orai1 mutants G98P and G98D), which closely packs its Cα carbon with the side chain of Phe 171, result in channels that are constitutively conductive and demonstrate altered ion selectivity (26, 32). The close packing in the hydrophobic region suggests that the functional abnormalities of these mutants may be due to reduced structural integrity and/or slightly altered packing in the pore.

Below the hydrophobic region in Figure 3B and near the intracellular side of the membrane, the pore is lined by three basic residues from each subunit (Lys 163, Lys 159 and Arg 155) that are conserved as lysine or arginine among Orai orthologs (fig. S1). The eighteen lysine or arginine residues that line this portion of the pore create an unexpected environment for the pore of a channel that conducts cations (Fig. 3D). The M1 helix is slightly bent at Ser 162 and is enriched for residues that are often associated with bends in helices (serine, threonine and glycine) in the region that spans the junction between the hydrophobic and basic portions of the pore (Fig. 3A, fig. S4). This raises the possibility that the conformation of the basic region could change, perhaps as part of the gating process, while the hydrophobic section and glutamate ring remain fairly fixed.

External Ca^{2+} binding and ion selectivity

In crystals soaked in Ca^{2+}, electron density consistent with a Ca^{2+} ion is observed on the extracellular side of the glutamate ring (in what we term the external site) (Fig. 4A). Because it is difficult to distinguish Ca^{2+} from other ions or water molecules in electron density maps, we collected diffraction data from a crystal soaked in barium (Ba^{2+}), which permeates through the CRAC channel (22, 33), and can be identified in electron density maps from its anomalous diffraction signal. The anomalous difference electron density map contained a 10 σ peak for Ba^{2+} in the external site, consistent with the assessment that it is a binding site for Ca^{2+} (Fig. 4A). Ba^{2+} is positioned slightly farther away from the glutamate ring than Ca^{2+} and this correlates with the ionic radii of the ions (1.35 Å for Ba^{2+} and 0.99 Å for Ca^{2+}). It is possible that the ion coordination, which could be either direct or water-mediated, is not six-fold symmetric due to the flexibility of glutamate side chains. The backbone carbonyl oxygen of Glu 178 at the C-terminal end of M1 might also contribute to Ca^{2+} binding (Fig. 4A). To investigate if Gd^{3+} blocks the channel by binding to the same site, diffraction data were collected from crystals soaked in Gd^{3+}, which also has a strong anomalous diffraction signal. The anomalous difference electron density map showed a 14 σ peak for Gd^{3+} in the external site (Fig. 4B). The density is positioned closer to the glutamate ring than for Ca^{2+} and this may be indicative of the high affinity of Gd^{3+} and its +3 charge. Notably, the single Ca^{2+} binding site identified is located just outside the pore rather than within it. This configuration of ion binding distinguishes Orai from K^+ channels, which have multiple ions present within the pore in their structures (34), and this likely reflects differences in the mechanisms for ion permeation and selectivity.

CRAC channels may achieve their exquisite Ca^{2+} selectivity by high-affinity binding of Ca^{2+} to the glutamate ring that likely constitutes the ion selectivity filter. Accordingly, mutation of the glutamate (Glu 178 in Orai or Glu 106 in Orai1) to aspartic acid dramatically increases the channel's permeability to monovalent cations (8-10, 13). Because the ionic radii of Ca^{2+} and Na^{+} are nearly identical (0.99 Å and 0.95 Å, respectively), selectivity for Ca^{2+} is most likely due to the ion's greater positive charge. Consistent with this trend, we observe that high affinity blockage of Orai by the trivalent lanthanide Gd^{3+} is due to binding in the external site.

Identification of the external site raises the question of whether there is only one Ca^{2+} binding site or if there are other site(s) that are occupied during permeation. In Orai, the Ca^{2+} permeation rate (up to ~ 10^4 ions per second (35, 36)) is much slower than the rate at which Ca^{2+} ions would diffuse to the extracellular mouth of the pore (~ 10^6 ions per second at physiological [Ca^{2+}] (37)) and so a single high-affinity Ca^{2+} binding site with a fast on-rate (from the extracellular solution) and a slow off-rate (into the pore) might be able to account for Ca^{2+}-selective permeation. However, some evidence, including an anomalous mole fraction effect (33), suggests that there may be more than one Ca^{2+} binding site. A second binding site might account for the property that while Na^{+} currents through CRAC channels are blocked by micromolar concentrations of Ca^{2+}, Ca^{2+} does not appreciably flow until the external solution contains millimolar concentrations of it (19, 20). Additionally, the extent of blockage of Na^{+} current at micromolar levels of Ca^{2+} is dependent on the voltage applied across the membrane (~ 10% block at -20 mV and ~ 50% block at -80 mV with 20 μM external Ca^{2+}) (36, 38), which suggests that an ion binding site is located within the voltage gradient, whereas the external site would probably be located outside of it.

If a second binding site in the selectivity filter for Ca^{2+} exists, we expect that it would be located just below the glutamate ring. This hypothetical internal site, which might only be occupied transiently during permeation, would reside within a voltage field across the membrane and may explain the voltage-dependence for block of Na^{+} current by Ca^{2+}. The binding of a Ca^{2+} ion in the external site could displace a Ca^{2+} ion from the internal site due to electrostatic repulsion between the ions, thereby allowing selective Ca^{2+} permeation.

Anion binding in the basic region of the pore

Electron density maps have strong density in the basic region of the pore that appears to plug it. The anomalous difference electron density was also strong in this site (up to 20 σ), aiding the identification of the bound atom(s) (Fig. 5A). The density cannot be due to the surrounding protein side chains because they would have negligible anomalous scattering and the components of the crystallization solution did not contain elements that would give a strong anomalous signal. To identify possible metal ions that might have co-purified with Orai, the protein sample was analyzed by inductively coupled plasma - mass spectrometry (ICP-MS) and was found to contain ~ 0.6 molar equivalents of iron and ~ 0.1 molar equivalents of zinc (Table S2), both of which have anomalous scattering properties. Anomalous scattering data collected using λ=1.735 Å X-rays, slightly shorter than the absorption edge for iron (1.7433 Å) where the anomalous signal from iron would be strong (*f”* ~ 3.9 e), yielded a 20 σ peak in the anomalous difference map (Table 1). Using λ=1.900 Å X-rays, where the anomalous signal from iron would be weaker (*f”* ~ 0.5 e), the peak was 5 σ. F_o-F_c electron density maps calculated from these datasets had comparable (~10 σ) peaks, indicating that the difference in the strength of the anomalous signal was not due to differing occupancies of the bound entity between the crystals. Datasets collected above and below the absorption edge for zinc (λ=1.284 Å) yielded comparable anomalous difference density in the pore, but indicated that zinc was bound in a crystal contact (fig. S6). We

therefore conclude that a major species bound in the basic region of the pore contains iron, which was present in the media used for cell growth.

Because this region of the pore is highly basic, we tested whether it could bind anions by soaking crystals in the complex anion iridium hexachloride, $(IrCl_6)^{3-}$. Diffraction data were collected using λ=1.1033 Å X-rays to optimize the anomalous diffraction signal from iridium (*f*”~ 10.1 e), where it would be stronger than that for iron (*f*”~ 1.8 e, Table 1). The anomalous difference electron density map contained two peaks in the basic region: a 29 σ peak for $(IrCl_6)^{3-}$ between Lys 163 and Lys 159 and an 8 σ peak adjacent to Arg 155. Otherwise, the overall structure of Orai complexed with $(IrCl_6)^{3-}$ was indistinguishable from the native structure. We conclude that the basic region can bind anion(s). Because we observe iron in this anion binding site, we speculate that it is also bound in the form of a complex anion or mediated by counter ions. In support of this, hexachloroferrate anions, $(FeCl_6)^{3-}$, are known to be stabilized by hydrogen bond interactions with amines (39). Although possible, it seems unlikely that iron binds within the pore in a physiological setting because of the limited amount of iron freely available within cells. More likely, the basic region of the pore binds available intracellular anion(s), with possible candidates being a sulfate or phosphate species (phosphate, pyrophosphate, etc.).

The K163W mutant

The crystal structure of the non-conductive K163W mutant gives further insight into the basic region of the pore. The overall structure of the K163W mutant is indistinguishable (at the current resolution) from the structure with the wild-type pore (root mean square deviation for Cα atoms is 0.1 Å). The only discernable difference with regard to the protein is that the side chain of the tryptophan residue at position 163 projects into the pore (Fig. 5C). The six tryptophan residues, one from each subunit, are tightly packed and extend the hydrophobic region of the pore an additional helical turn.

Electron density maps for the K163W mutant did not contain the anomalous difference density within the pore ascribed to iron. Accordingly, ICP-MS analysis of the K163W mutant protein indicated that it contained only about one third as much iron (Table S2). Lys 159 and Arg 155 have less well-defined electron density in the mutant, presumably because of the absence of an anion. To explore the effect of the K163W mutant on the ability of the pore to bind anions, we calculated an anomalous difference electron density map from a crystal soaked in $(IrCl_6)^{3-}$, and found that its distribution in the pore is different than for the wild-type pore. For the K163W mutant, a single peak (12 σ) was observed in the pore, located between Lys 159 and Arg 155 (Fig. 5D), indicating that the mutant eliminates one of the anion binding sites.

Ion permeation and gating

Flux assays indicate that the pore of $Orai_{cryst}$ is closed, as would be expected prior to activation by STIM (Fig 1). Because of the narrow width of the basic region of the pore (Fig. 3B) and its extreme positive charge, we suspect that this section is not permeable to Ca^{2+} in its current conformation and forms a closed gate. Hydrophobic amino acids substituted for Lys 163 (Arg 91 in human Orai1), within the basic region, prevent channel activation (40). The structure of the K163W mutant indicates that the tryptophan residues make extensive hydrophobic interactions with each other and that the mutation eliminates one of the anion binding sites. Anion(s) bound in the basic region of a wild-type pore would likely occlude the pore and help stabilize the closed conformation. Whereas the hydrophobic packing in the mutants would probably be static, locking the channel in a closed conformation, an anion bound at Lys 163 could dissociate, allowing the wild-type pore to open.

The structure suggests that the glutamate ring and hydrophobic section regions are permeable to Ca^{2+} in the observed conformation. The distance between the oxygen atoms of the glutamate ring and the central axis of the pore is ~ 3 Å, which is similar to the typical coordination distance between Ca^{2+} and oxygen in crystal structures of Ca^{2+}-binding proteins (~ 2.4 Å) (41). This suggests that a Ca^{2+} ion would pass through the glutamate ring by coordinating the side chain oxygen atoms directly and becoming at least partially dehydrated. After emerging from the glutamate ring, the permeating Ca^{2+} ion would likely coordinate additional waters within the hydrophobic section. In support of this hypothesis, electron density consistent with water molecules is present within the hydrophobic section (fig. S5).

Experiments suggest that a cytosolic portion of STIM interacts with Orai to activate the channel (24, 42-44) and that the interaction involves N- and C-terminal regions of Orai that correspond to the cytosolic region of M1 and the M4 extension in the structure (23, 24, 27-29, 45). Deletion of the M4 extension or mutation of the residues that are observed to mediate its coiled-coil packing (Ile 316 or Leu 319, corresponding to Leu 273 and Leu 276 in human Orai1) disrupts STIM binding and channel activation (23, 24, 27-29). This raises the possibility that STIM, which contains regions predicted to form coiled-coils, binds to the M4 extension by substituting for the coiled-coil interaction observed between the Orai subunits and that the arrangement of the M4 extensions in the structure is a quiescent one prior to STIM binding. While C-terminal modifications of Orai disrupt STIM binding, deletion of the cytosolic portion of M1 or certain mutations within it (including the Orai1 mutants R91W and Lys 85, which faces away from the pore, to glutamate) have little effect on STIM binding but prevent channel activation (23, 24, 45). These observations are consistent with a hypothesis proposed by Park *et* al. that STIM binding provides the energy for channel gating by bridging the N- and C-termini of the channel (24).

Based on the structure and the available functional data, we constructed a working model for an open conformation of the channel (Fig. 6). In it, the M4 extension helices project (> 50 Å) into the cytosol and interact with a cytosolic portion of STIM. The basic region of the pore is dilated by the outward bending of the M1 helices (modeled to occur between Ser 161 and Gly 170), which interact via their N-terminal regions with STIM. The M2-M3 loops (amino acids 220-235), while disordered in the current structure, might also make contributions given their intracellular location and significant conservation (fig. S1). The dilation of the pore is expected to reduce the affinity of the basic region for anion(s), allowing them to be displaced.

Discussion

The crystal structure of Orai reveals an architecture that appears well suited for its physiological role. The ~ 10,000 fold resting concentration gradient of Ca^{2+} across the plasma membrane (~ 1 mM extracellular and ~ 100 nM intracellular [Ca^{2+}]) must be maintained to prevent aberrant Ca^{2+} signaling within cells, and therefore Orai must be tightly sealed shut when it is closed. Anion(s) bound in the basic region probably help serve this purpose. In an open conformation, the basic region would tend to prevent the permeation of cations that have modest concentration gradients (such as K^+ and Na^+, which have ~ 50 fold gradients) and in this way it would contribute to Ca^{2+}-selective permeation under physiological conditions. In order to establish a slow permeation rate that prevents overloading of the cell with Ca^{2+} and allows for fine tuning of sustained Ca^{2+} signals, the channel imposes energy barriers to ion permeation, which could include dissociation of Ca^{2+} from the selectivity filter (into the pore), permeation through the hydrophobic section, and electrostatic repulsion by the basic section. Ultimately, the channel's design takes advantage

of the large Ca^{2+} gradient across the plasma membrane, while tightly regulating the flow of Ca^{2+} into the cell to mediate one of the most fundamental types of signaling in cell biology.

Supplementary Material

Refer to Web version on PubMed Central for supplementary material.

References and Notes

1. Hogan PG, Lewis RS, Rao A. Molecular basis of calcium signaling in lymphocytes: STIM and ORAI. Annu. Rev. Immunol. 2010; 28:491. doi:10.1146/annurev.immunol.021908.132550 Medline. [PubMed: 20307213]
2. Roos J, et al. STIM1, an essential and conserved component of store-operated Ca^{2+} channel function. J. Cell Biol. 2005; 169:435. doi:10.1083/icb.200502019 Medline. [PubMed: 15866891]
3. Zhang SL, et al. STIM1 is a Ca^{2+} sensor that activates CRAC channels and migrates from the Ca^{2+} store to the plasma membrane. Nature. 2005; 437:902. doi:10.1038/nature04147 Medline. [PubMed: 16208375]
4. Liou J, et al. STIM is a Ca^{2+} sensor essential for Ca^{2+}-store-depletion-triggered Ca^{2+} influx. Curr. Biol. 2005; 15:1235. doi:10.1016/i.cub.2005.05.055 Medline. [PubMed: 16005298]
5. Feske S, et al. A mutation in Orai1 causes immune deficiency by abrogating CRAC channel function. Nature. 2006; 441:179. doi:10.1038/nature04702 Medline. [PubMed: 16582901]
6. Vig M, et al. CRACM1 is a plasma membrane protein essential for store-operated Ca^{2+} entry. Science. 2006; 312:1220. doi:10.1126/science.1127883 Medline. [PubMed: 16645049]
7. Zhang SL, et al. Genome-wide RNAi screen of Ca^{2+} influx identifies genes that regulate Ca^{2+} release-activated Ca^{2+} channel activity. Proc. Natl. Acad. Sci. U.S.A. 2006; 103:9357. doi:10.1073/pnas.0603161103 Medline. [PubMed: 16751269]
8. Yeromin AV, et al. Molecular identification of the CRAC channel by altered ion selectivity in a mutant of Orai. Nature. 2006; 443:226. doi:10.1038/nature05108 Medline. [PubMed: 16921385]
9. Prakriya M, et al. Orai1 is an essential pore subunit of the CRAC channel. Nature. 2006; 443:230. doi:10.1038/nature05122 Medline. [PubMed: 16921383]
10. Vig M, et al. CRACM1 multimers form the ion-selective pore of the CRAC channel. Curr. Biol. 2006; 16:2073. doi:10.1016/i.cub.2006.08.085 Medline. [PubMed: 16978865]
11. Single-letter abbreviations for the amino acid residues are as follows: A, Ala; C, Cys; D, Asp; E, Glu; F, Phe; G, Gly; H, His; I, Ile; K, Lys; L, Leu; M, Met; N, Asn; P, Pro; Q, Gln; R, Arg; S, Ser; T, Thr; V, Val; W, Trp; and Y, Tyr.
12. Carrasco S, Meyer T. STIM proteins and the endoplasmic reticulum-plasma membrane junctions. Annu. Rev. Biochem. 2011; 80:973. doi:10.1146/annurev-biochem-061609-165311 Medline. [PubMed: 21548779]
13. McNally BA, Yamashita M, Engh A, Prakriya M. Structural determinants of ion permeation in CRAC channels. Proc. Natl. Acad. Sci. U.S.A. 2009; 106:22516. doi:10.1073/pnas.0909574106 Medline. [PubMed: 20018736]
14. Zhou Y, Ramachandran S, Oh-Hora M, Rao A, Hogan PG. Pore architecture of the ORAI1 store-operated calcium channel. Proc. Natl. Acad. Sci. U.S.A. 2010; 107:4896. doi:10.1073/pnas.1001169107 Medline. [PubMed: 20194792]
15. Penna A, et al. The CRAC channel consists of a tetramer formed by Stim-induced dimerization of Orai dimers. Nature. 2008; 456:116. doi:10.1038/nature07338 Medline. [PubMed: 18820677]
16. Ji W, et al. Functional stoichiometry of the unitary calcium-release-activated calcium channel. Proc. Natl. Acad. Sci. U.S.A. 2008; 105:13668. doi:10.1073/Dnas.0806499105 Medline. [PubMed: 18757751]
17. Mignen OJL, Thompson TJ. Shuttleworth, Orai1 subunit stoichiometry of the mammalian CRAC channel pore. J. Physiol. 2008; 586:419. doi:10.1113/iphysiol.2007.147249 Medline. [PubMed: 18006576]

18. Demuro A, et al. Subunit stoichiometry of human Orai1 and Orai3 channels in closed and open states. Proc. Natl. Acad. Sci. U.S.A. 2011; 108:17832. doi:10.1073/pnas.1114814108 Medline. [PubMed: 21987805]
19. Hoth M, Penner R. Calcium release-activated calcium current in rat mast cells. J. Physiol. 1993; 465:359. Medline. [PubMed: 8229840]
20. Lepple-Wienhues A, Cahalan MD. Conductance and permeation of monovalent cations through depletion-activated Ca^{2+} channels (ICRAC) in Jurkat T cells. Biophys. J. 1996; 71:787. doi: 10.1016/S0006-3495(96)79278-0 Medline. [PubMed: 8842217]
21. Aussel C, Marhaba R, Pelassy C, Breittmayer JP. Submicromolar La^{3+} concentrations block the calcium release-activated channel, and impair CD69 and CD25 expression in CD3- or thapsigargin-activated Jurkat cells. Biochem. J. 1996; 313:909. Medline. [PubMed: 8611174]
22. Yeromin AV, Roos J, Stauderman KA, Cahalan MD. A store-operated calcium channel in *Drosophila* S2 cells. J. Gen. Physiol. 2004; 123:167. doi:10.1085/igp.200308982 Medline. [PubMed: 14744989]
23. Li Z, et al. Mapping the interacting domains of STIM1 and Orai1 in Ca^{2+} release-activated Ca^{2+} channel activation. J. Biol. Chem. 2007; 282:29448. doi:10.1074/ibc.M703573200 Medline. [PubMed: 17702753]
24. Park CY, et al. STIM1 clusters and activates CRAC channels via direct binding of a cytosolic domain to Orai1. Cell. 2009; 136:876. doi:10.1016/i.cell.2009.02.014 Medline. [PubMed: 19249086]
25. Zhou Y, et al. STIM1 gates the store-operated calcium channel ORAI1 in vitro. Nat. Struct. Mol. Biol. 2010; 17:112. doi:10.1038/nsmb.1724 Medline. [PubMed: 20037597]
26. McNally BA, Somasundaram A, Yamashita M, Prakriya M. Gated regulation of CRAC channel ion selectivity by STIM1. Nature. 2012; 482:241. Medline. [PubMed: 22278058]
27. Navarro-Borelly L, et al. STIM1-Orai1 interactions and Orai1 conformational changes revealed by live-cell FRET microscopy. J. Physiol. 2008; 586:5383. doi:10.1113/iphysiol.2008.162503 Medline. [PubMed: 18832420]
28. Muik M, et al. Dynamic coupling of the putative coiled-coil domain of ORAI1 with STIM1 mediates ORAI1 channel activation. J. Biol. Chem. 2008; 283:8014. doi:10.1074/ibc.M708898200 Medline. [PubMed: 18187424]
29. Frischauf I, et al. Molecular determinants of the coupling between STIM1 and Orai channels: Differential activation of Orai1-3 channels by a STIM1 coiled-coil mutant. J. Biol. Chem. 2009; 284:21696. doi:10.1074/ibc.M109.018408 Medline. [PubMed: 19506081]
30. Doyle DA, et al. The structure of the potassium channel: Molecular basis of K^+ conduction and selectivity. Science. 1998; 280:69. doi:10.1126/science.280.5360.69 Medline. [PubMed: 9525859]
31. Aspartate residues on the disordered M1-M2 loop (D182 and D184, corresponding to DUO and D112 in Orail) probably also contribute to the acidic nature of the extracellular mouth of the pore.
32. Zhang SL, et al. Mutations in Orai1 transmembrane segment 1 cause STIM1-independent activation of Orai1 channels at glycine 98 and channel closure at arginine 91. Proc. Natl. Acad. Sci. U.S.A. 2011; 108:17838. doi:10.1073/pnas.1114821108 Medline. [PubMed: 21987804]
33. Hoth M. Calcium and barium permeation through calcium release-activated calcium (CRAC) channels. Pflugers Arch. 1995; 430:315. doi:10.1007/BF00373905 Medline. [PubMed: 7491254]
34. Zhou Y, Morais-Cabral JH, Kaufman A, MacKinnon R. Chemistry of ion coordination and hydration revealed by a K^+ channel-Fab complex at 2.0 A resolution. Nature. 2001; 414:43. doi: 10.1038/35102009 Medline. [PubMed: 11689936]
35. Zweifach A, Lewis RS. Mitogen-regulated Ca^{2+} current of T lymphocytes is activated by depletion of intracellular Ca^{2+} stores. Proc. Natl. Acad. Sci. U.S.A. 1993; 90:6295. doi:10.1073/pnas. 90.13.6295 Medline. [PubMed: 8392195]
36. Prakriya M, Lewis RS. Regulation of CRAC channel activity by recruitment of silent channels to a high open-probability gating mode. J. Gen. Physiol. 2006; 128:373. doi:10.1085/igp.200609588 Medline. [PubMed: 16940559]
37. Hille, B. Ionic Channels of Excitable Membranes. ed. 2. Sinauer Associates; Sunderland, MA: 1992. p. xiii

38. Bakowski D, Parekh AB. Monovalent cation permeability and Ca^{2+} block of the store-operated Ca^{2+} current I_{CRAC} in rat basophilic leukemia cells. Pflugers Arch. 2002; 443:892. doi:10.1007/s00424-001-0775-8 Medline. [PubMed: 11889590]
39. James BD, et al. The hexachloroferrate(III) anion stabilized in hydrogen bonded packing arrangements. A comparison of the x-ray crystal structures and low temperature magnetism of tetrakis (methylammonium) hexachloroferrate (III) chloride (I) and tetrakis (hexamethylenediammonium) hexachloroferrate (III) tetrachloroferrate (III) tetrachloride (II). Inorg. Chim. Acta. 1996; 247:169. doi:10.1016/0020-1693(95)04955-X.
40. Derler I, et al. Increased hydrophobicity at the N terminus/membrane interface impairs gating of the severe combined immunodeficiency-related ORAI1 mutant. J. Biol. Chem. 2009; 284:15903. doi:10.1074/ibc.M808312200 Medline. [PubMed: 19366689]
41. Kawasaki H, Kretsinger RH. Calcium-binding proteins 1: EF-hands. Protein Profile. 1995; 2:297. Medline. [PubMed: 7553064]
42. Yuan JP, et al. SOAR and the polybasic STIM1 domains gate and regulate Orai channels. Nat. Cell Biol. 2009; 11:337. doi:10.1038/ncb1842 Medline. [PubMed: 19182790]
43. Muik M, et al. A cytosolic homomerization and a modulatory domain within STIM1 C terminus determine coupling to ORAI1 channels. J. Biol. Chem. 2009; 284:8421. doi:10.1074/ibc.C800229200 Medline. [PubMed: 19189966]
44. Kawasaki T, Lange I, Feske S. A minimal regulatory domain in the C terminus of STIM1 binds to and activates ORAI1 CRAC channels. Biochem. Biophys. Res. Commun. 2009; 385:49. [PubMed: 19433061]
45. Lis A, Zierler S, Peinelt C, Fleig A, Penner R. A single lysine in the N-terminal region of store-operated channels is critical for STIMl-mediated gating. J. Gen. Physiol. 2010; 136:673. doi:l0.l085/igp.201010484 Medline. [PubMed: 21115697]
46. Kawate T, Gouaux E. Fluorescence-detection size-exclusion chromatography for precrystallization screening of integral membrane proteins. Structure. 2006; 14:673. doi:10.1016/i.str.2006.01.013 Medline. [PubMed: 16615909]
47. Kilmartin JV, Wright B, Milstein C. Rat monoclonal antitubulin antibodies derived by using a new nonsecreting rat cell line. J. Cell Biol. 1982; 93:576. doi:l0.l083/icb.93.3.576 Medline. [PubMed: 6811596]
48. Long SB, Campbell EB, MacKinnon R. Crystal structure of a mammalian voltage-dependent Shaker family K^+ channel. Science. 2005; 309:897. doi:10.1126/science.1116269 Medline. [PubMed: 16002581]
49. Otwinowski Z, Minor W. Processing of x-ray diffraction data collected in oscillation mode. Methods Enzymol. 1997; 276:307. doi:10.1016/S0076-6879(97)76066-X.
50. Vonrhein C, Blanc E, Roversi P, Bricogne G. Automated structure solution with autoSHARP. Methods Mol. Biol. 2007; 364:215. Medline. [PubMed: 17172768]
51. Cowtan KD. Joint CCP4 and ESF-EACBM Newsletter on Protein Crystallography. 1994; (31):34–38.
52. Jones TA, Zou J-Y, Cowan SW, Kjeldgaard M. Improved methods for building protein models in electron density maps and the location of errors in these models. Acta Crystallogr. A. 1991; 47:110. doi:10.1107/S0108767390010224 Medline. [PubMed: 2025413]
53. Emsley P, Lohkamp B, Scott WG, Cowtan K. Features and development of Coot. Acta Crystallogr. D Biol. Crystallogr. 2010; 66:486. doi:10.1107/S0907444910007493 Medline.
54. Briinger AT, et al. Crystallography & NMR system: A new software suite for macromolecular structure determination. Acta Crystallogr. D Biol. Crystallogr. 1998; 54:905. doi:10.1107/S0907444998003254 Medline. [PubMed: 9757107]
55. Adams PD, et al. PHENIX: A comprehensive Python-based system for macromolecular structure solution. Acta Crystallogr. D Biol. Crystallogr. 2010; 66:213. doi:10.1107/S0907444909052925 Medline. [PubMed: 20124702]
56. Smart OS, Neduvelil JG, Wang X, Wallace BA, Sansom MS. HOLE: A program for the analysis of the pore dimensions of ion channel structural models. J. Mol. Graph. 1996; 14:354, 376. doi:10.1016/S0263-7855(97)00009-X Medline. [PubMed: 9195488]

57. Baker NA, Sept D, Joseph S, Holst MJ, McCammon JA. Electrostatics of nanosystems: Application to microtubules and the ribosome. Proc. Natl. Acad. Sci. U.S.A. 2001; 98:10037. doi: 10.1073/pnas.181342398 Medline. [PubMed: 11517324]
58. Heginbotham L, Kolmakova-Partensky L, Miller C. Functional reconstitution of a prokaryotic K^+ channel. J. Gen. Physiol. 1998; 111:741. doi:10.1085/igp.111.6.741 Medline. [PubMed: 9607934]
59. Zhang J, Feng Y, Forgac M. Proton conduction and bafilomycin binding by the VO domain of the coated vesicle V-ATPase. J. Biol. Chem. 1994; 269:23518. Medline. [PubMed: 8089118]
60. Lee S-Y, Letts JA, MacKinnon R. Functional reconstitution of purified human Hvl H^+ channels. J. Mol. Biol. 2009; 387:1055. doi:10.1016/i.imb.2009.02.034 Medline. [PubMed: 19233200]
61. Feng L, Campbell EB, Hsiung Y, MacKinnon R. Structure of a eukaryotic CLC transporter defines an intermediate state in the transport cycle. Science. 2010; 330:635. doi:10.1126/science.1195230 Medline. [PubMed: 20929736]
62. Miller AN, Long SB. Crystal structure of the human two-pore domain potassium channel K2P1. Science. 2012; 335:432. doi:10.1126/science.1213274 Medline. [PubMed: 22282804]
63. Hayashi Y, Matsui H, Takagi T. Membrane protein molecular weight determined by low-angle laser light-scattering photometry coupled with high-performance gel chromatography. Methods Enzymol. 1989; 172:514. doi:10.1016/S0076-6879(89)72031-0 Medline. [PubMed: 2546016]
64. Yernool D, Boudker O, Folta-Stogniew E, Gouaux E. Trimeric subunit stoichiometry of the glutamate transporters from *Bacillus caldotenax* and *Bacillus stearothermophilus*. Biochemistry. 2003; 42:12981. doi:10.1021/bi030161a Medline. [PubMed: 14596613]
65. Folta-Stogniew E. Oligomeric states of proteins determined by size-exclusion chromatography coupled with light scattering, absorbance, and refractive index detectors. Methods Mol. Biol. 2006; 328:97. Medline. [PubMed: 16785643]
66. Folta-Stogniew E, Williams KR. Determination of molecular masses of proteins in solution: Implementation of an HPLC size exclusion chromatography and laser light scattering service in a core laboratory. J. Biomol. Tech. 1999; 10:51. Medline. [PubMed: 19499008]
67. Ballesteros JA, Deupi X, Olivella M, Haaksma EE, Pardo L. Serine and threonine residues bend α-helices in the $\chi 1 = g^-$ conformation. Biophys. J. 2000; 79:2754. doi:10.1016/S0006-3495(00)76514-3 Medline. [PubMed: 11053148]
68. Jiang Y, et al. The open pore conformation of potassium channels. Nature. 2002; 417:523. doi: 10.1038/417523a Medline. [PubMed: 12037560]
69. Alam A, Jiang Y. High-resolution structure of the open NaK channel. Nat. Struct. Mol. Biol. 2008; 16:30. doi:10.1038/nsmb.1531 Medline. [PubMed: 19098917]

One sentence summary

The structure of a channel that generates intracellular calcium signals reveals a hexameric assembly and an unusual ion pore.

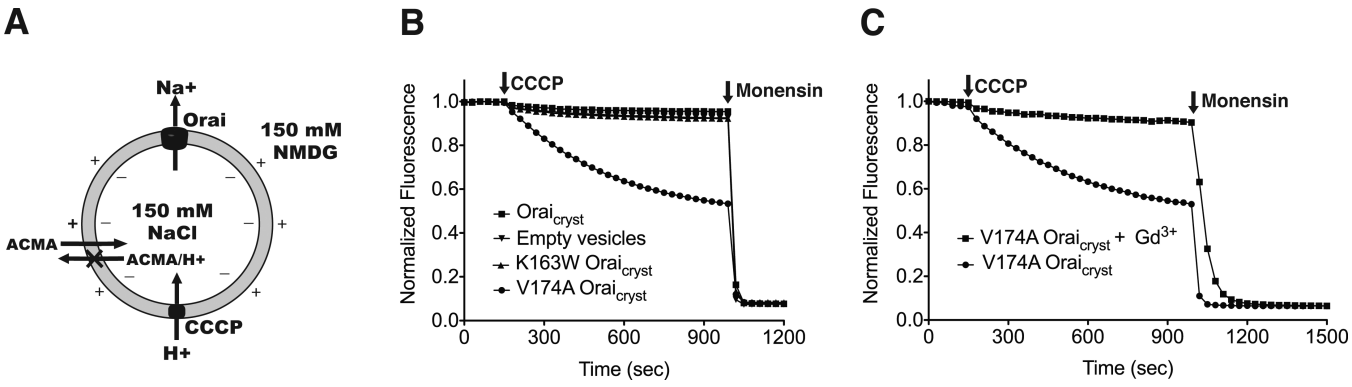

Fig. 1.

Channel reconstitution in liposomes. (**A)** Schematic of the fluorescence-based flux assay. Vesicles containing Orai or those prepared without protein (empty vesicles) were loaded with 150 mM NaCl and diluted 100-fold into flux buffer containing a fluorescent pH indicator (ACMA) and 150 mM n-methyl-d-glucamine (NMDG) to establish a Na^+ gradient. After stabilization of the fluorescence signal (150 sec) a proton ionophore (CCCP) was added to the sample, and an electrical potential arising from Na^+ efflux was used to drive the uptake of protons into the vesicles, which quenches the fluorescence of ACMA. The "X" indicates that ACMA is no longer membrane permeable in the protonated form. (**B)** Fluorescence measurements for the indicated protein constructs of Orai. Monensin, a Na^+ ionophore, was added after 990 seconds to render all vesicles permeable to Na^+ and establish a minimum fluorescence baseline. Fluorescence was normalized by dividing by the initial value. (**C)** Fluorescence trace observed for V174A $Orai_{cryst}$ in the absence and presence of Gd^{3+}.

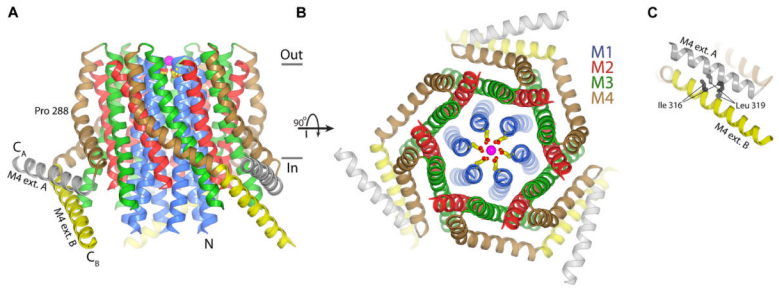

Fig. 2.

Architecture of Orai. (**A**) A ribbon representation showing the tertiary structure of the channel from the side. The helices are colored: M1 (blue), M2 (red), M3 (green), M4 (brown), M4 extension (yellow in subunit A and grey in subunit B). Also shown are a Ca^{2+} ion (magenta sphere) and the nearby Glu 178 residues (yellow sticks). Based on the hydrophobic region of the channel's surface, horizontal lines (~ 30 Å apart) suggest approximate boundaries of the inner (In) and outer (Out) leaflets of the membrane. (**B**) An orthogonal view of the channel from the extracellular side. **(C)** Close-up view showing the interaction between the M4 extension helices.

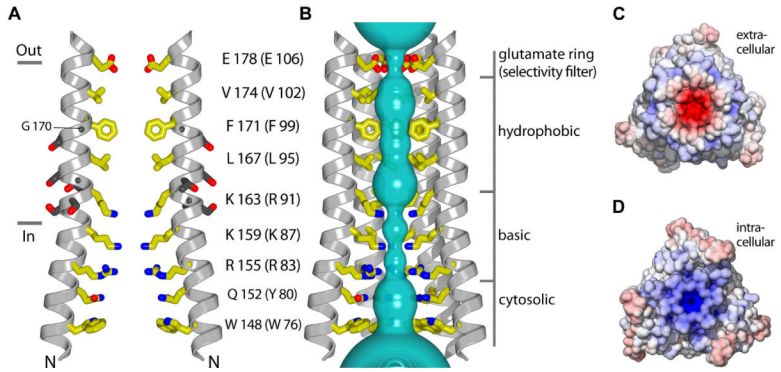

Fig. 3.

Ion pore. (**A**) Two M1 helices are drawn (four are omitted for clarity), showing the amino acids lining the pore in yellow. The approximate boundaries of the membrane-spanning region are shown as horizontal lines. In parentheses are the corresponding amino acids in human Orai1. Ser 161, Ser 162, Thr 164, Ser 165, Ser 169 and Gly 170 are drawn as grey sticks. (**B**) View of the pore. Within a ribbon representation of four M1 helices (two in the foreground are removed for clarity) is a representation (teal color) of the minimal radial distance from the center to the nearest van der Waals protein contact. The sections of the pore discussed in the text are labeled. **(C)** and **(D)** Molecular surface of Orai viewed from the extracellular (C) and intracellular (D) sides and colored according to the electrostatic potential contoured from -10 kT (red) to +10 kT (blue) (dielectric constant: 80).

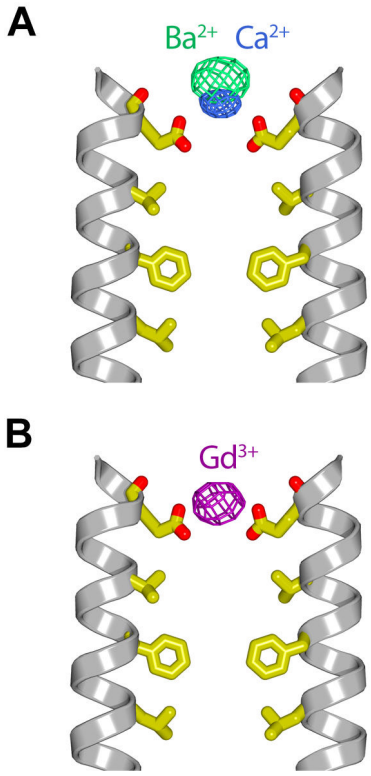

Fig. 4.

Cation binding in the external site. (**A**) Ba^{2+} and Ca^{2+} binding. The glutamate ring and hydrophobic section of the pore are depicted as in Fig. 3A. Anomalous difference electron density for Ba^{2+} is shown in green mesh (calculated from 20 – 5 Å resolution using phases derived from the final model and contoured at 6 σ from a diffraction dataset collected using λ = 1.70 Å X-rays and a crystal soaked in 50 mM $BaCl_2$). Electron density corresponding to Ca^{2+} is shown from a simulated annealing F_o-F_c omit map (blue mesh, calculated from 20 – 3.8 Å resolution and contoured at 4 σ) from a crystal soaked in 50 mM $CaCl_2$ (Table S1). The backbone carbonyl oxygen of Glu 178 is also shown in stick representation. (**B**) Gd^{3+} binding. Anomalous difference electron density is shown in purple mesh from a crystal soaked in 1 mM $GdCl_3$ (calculated from 20 – 5 Å resolution using model phases and contoured at 11 σ from a diffraction dataset collected using λ = 1.70 Å X-rays).

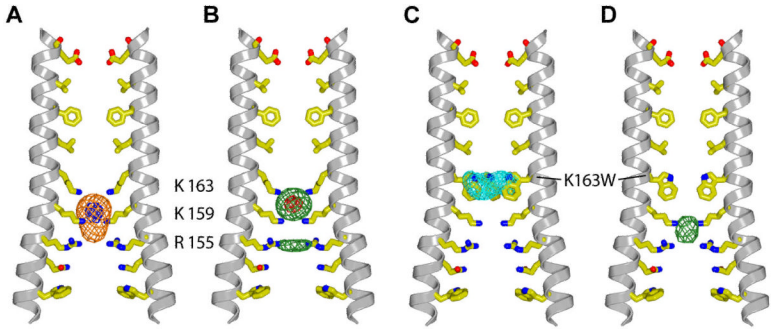

Fig. 5.

Anion binding and the K163W mutant. (**A**) Anomalous difference electron density in the basic region of the wild-type pore contoured at 7 σ (orange mesh) and 14 σ (blue mesh) from a native un-soaked crystal. The M1 helices are depicted as in Fig 3A. The map was calculated using phases derived from the protein model and a diffraction dataset collected using λ = 1.735 Å X-rays (resolution range 20 – 5 Å, Table 1). (**B**) Anomalous difference electron density present in the wild-type pore from a crystal soaked in $(IrCl_6)^{3-}$. The map is contoured at 7 σ (green mesh) and 20 σ (red mesh) (calculated using model phases from 20 - 5 Å resolution from a diffraction dataset collected using λ = 1.1033 Å X-rays). **(C)** and **(D)** The K163W mutant. Two M1 helices of the K163W mutant are depicted in the same manner as (A). (C) Electron density (blue mesh) is shown for the tryptophan side chains at residue 163 (represented as sticks). The density is from a simulated annealing F_o-F_c map in which the tryptophan side chains have been removed from the model (calculated from 20 to 3.35 Å resolution and contoured at 3 σ). (D) Anomalous difference electron density (green mesh) in the pore of a K163W mutant crystal soaked in $(IrCl_6)^{3-}$ (calculated from 20 - 5 Å resolution using model phases and contoured at 7 σ from a diffraction dataset collected using λ = 1.1033 Å X-rays).

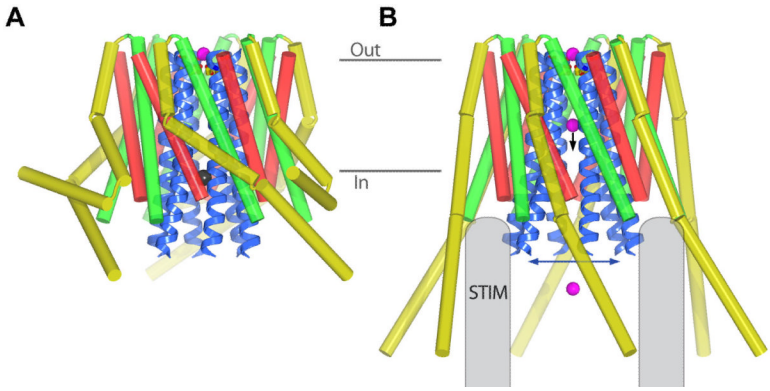

Fig. 6.

Observed structure and hypothetical open state. (**A**) Observed (apparently closed) structure of Orai. The view is from the side with the M1 helices drawn as blue ribbons and the other helices shown as cylinders (M2 colored red, M3 colored green, and M4 and M4 extension colored yellow). A Ca^{2+} ion in the external site is depicted as a magenta sphere; an anion in the basic region of the pore is depicted as a grey sphere. Approximate boundaries of the lipid membrane are shown as horizontal lines. (**B**) Hypothetical model of an open state. The pore is widened by the outward dilation of the M1 helices (blue arrow). A black arrow indicates that Ca^{2+} is able to move though the pore unobstructed. The intracellular ends of the M1 helices are hypothesized to interact with a cytosolic portion of STIM, as are the M4 extensions, which are modeled to protrude into the cytosol. The depiction of a cytosolic portion of STIM is meant to posit the hypothesis that it might bridge the cytosolic portions of the M1 helices and the M4/M4 extension helices and is not meant to imply a particular structure, oligomeric state, or stoichiometry with Orai.

Table 1

Electron density in the basic region using different X-ray wavelengths. Peak heights of the F_o-F_c and anomalous difference electron density maps within the basic region are indicated for diffraction datasets from crystals (native un-soaked crystals from the same protein preparation, and of comparable size and diffraction quality) that were collected at the indicated wavelengths. F_o-F_c maps were calculated using protein model phases (without ions in the pore) after rigid body refinement and using the resolution range 20 – 4 Å. Anomalous difference electron density maps were calculated using these phases and the resolution range 20 – 5 Å. Additional statistics are listed (table S3). The theoretical values for *f'* and *f"* (where the X-ray scattering factor $f = f_o + f' + if''$) were obtained from the skuld.bmsc.washington.edu/scatter website.

Wavelength (Å)	1.100	1.735	1.900
F_o-F_c peak height (σ)	9.5	9.0	10.6
Theoretical *f'* of iron (e)	0.1	-5.0	-2.2
Anomalous difference peak height (σ)	12.3	20.9	5.1
Theoretical *f"* of iron (e)	1.8	3.9	0.5